# Self-Organized Traveling Chemo-Hydrodynamic Fingers Triggered by a Chemical Oscillator

**ARTICLE** *in* JOURNAL OF PHYSICAL CHEMISTRY LETTERS · FEBRUARY 2014

Impact Factor: 7.46 · DOI: 10.1021/jz402625z

THE JOURNAL OF PHYSICAL CHEMISTRY Letters

Letter

pubs.acs.org/JPCL

# Self-Organized Traveling Chemo-Hydrodynamic Fingers Triggered by a Chemical Oscillator

D. M. Escala,*[,†] M. A. Budroni,*[,‡,§] J. Carballido-Landeira,*[,†,⊥] A. De Wit,*[,‡] and A. P. Muñuzuri*[,†]

[†]Nonlinear Physics Group, University of Santiago de Compostela, 15782 Santiago de Compostela, Spain

[‡]Nonlinear Physical Chemistry Unit, Service de Chimie Physique et Biologie Théorique, Faculté des Sciences, Université Libre de Bruxelles (ULB), CP231, 1050 Brussels, Belgium

Supporting Information

**ABSTRACT:** Pulsatile chemo-hydrodynamic patterns due to a coupling between an oscillating chemical reaction and buoyancy-driven hydrodynamic flows can develop when two solutions of separate reactants of the Belousov−Zhabotinsky reaction are put in contact in the gravity field and conditions for chemical oscillations are met in the contact zone. In regular oscillatory conditions, localized periodic changes in the concentration of intermediate species induce pulsatile density gradients, which, in turn, generate traveling convective fingers breaking the transverse symmetry. These patterns are the self-organized result of a genuine coupling between chemical and hydrodynamic modes.

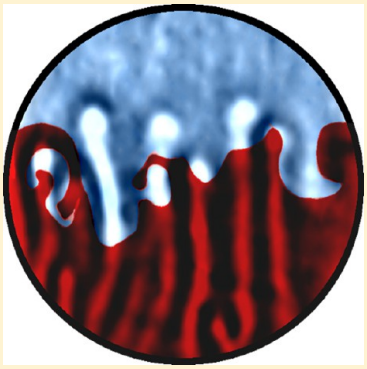

**SECTION:** Liquids; Chemical and Dynamical Processes in Solution

Out-of-equilibrium, breaking of symmetries and related spatiotemporal patterns have been much studied in hydrodynamic and reaction−diffusion (RD) systems.[1−3] At the intersection between these two fields, chemo-hydrodynamics focuses on analyzing patterns and instabilities that result from a nonlinear coupling of hydrodynamic and RD processes.[4] Related problems range from fingering instabilities of reactive interfaces[5,6] or traveling chemical fronts[4] to the spatiotemporal dynamics of chemicals advected in complex flow fields.[7,8] The reaction−diffusion−convection (RDC) interplay impacts numerous applications areas as diverse as combustion,[9] polymer processing,[10] extraction techniques[5,11] and $CO_2$ sequestration.[12]

When chemicals are passively slaved to the flow, the convective motions develop independently of the presence of reactive processes. On the other hand, in presence of active chemistry, the reactions modify a physical property of the fluid like its density, viscosity, or surface tension for instance. Concentration gradients in RD processes can then trigger unfavorable mobility gradients, which in turn can yield convection. As an example, even when starting from an initially stable density stratification of a less dense reactive solution on top of a denser one in the gravity field, chemical processes can trigger buoyancy-driven convection. This occurs when the reaction produces either a denser product locally or when differential diffusion phenomena implying the various chemicals[6,13−16] or heat and mass[17] come into play. The hydrodynamic patterns are then typically convective fingers growing vertically. Simple A+B→ C reactions have been shown to be able to break the up−down symmetry of such convective fingers.[13] More complex reactions prone to produce spatiotemporal RD structures can induce other synergetic combinations of chemical and hydrodynamic modes. Typical examples of such intrinsic chemo-hydrodynamic scenarios include reaction-driven convection around a traveling chemical front stably stratified from both solutal and thermal perspectives[4,17,18] and buoyancy or Marangoni-induced convective cells following chemical waves in excitable and oscillatory systems.[19−23] In such cases, the chemical kinetics drives the source of the convective flows, and the velocity field is different from what would be obtained in non reactive systems.

In this context, we provide here evidence that the self-organizing power of RD patterns can be used to control spatiotemporal dynamics of convective flows. Specifically, we show the existence of a novel chemo-hydrodynamic instability producing traveling convective fingers, the properties of which merge those of underlying RD traveling waves and buoyancy-driven flows. This self-organized chemo-hydrodynamic pattern is sustained by a chemical oscillator localized at the miscible interface between two solutions containing separated reactants of the Belousov−Zhabotinsky (BZ) reaction. In the dynamics, chemical concentration waves moving horizontally along the reactive interface (Figure 1a, upper row) couple to vertically

**Received:** December 3, 2013
**Accepted:** January 9, 2014

   dx.doi.org/10.1021/jz402625z | J. Phys. Chem. Lett. 2014, 5, 413−418

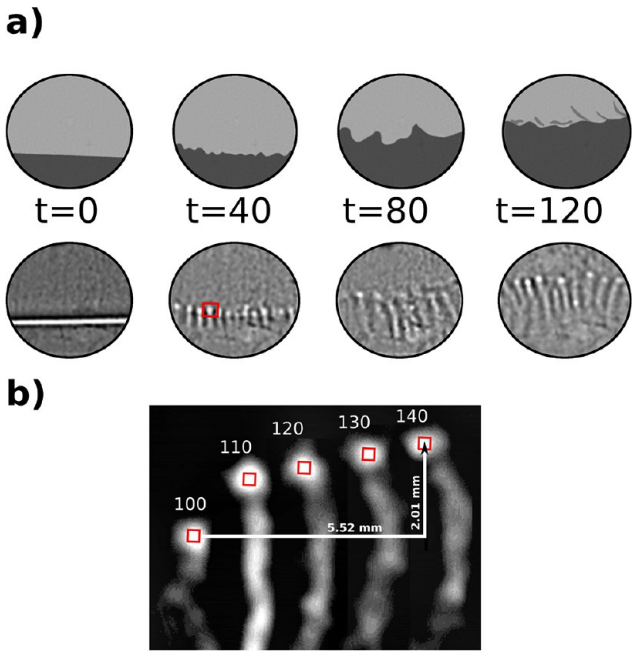


**Figure 1.** (a) Typical dynamics observed in the reactive zone in the chemical (upper row) and hydrodynamic (lower row) view when $[NaBrO_3]$ = 0.085 M. Dark and bright regions in the upper row correspond to the reduced and the oxidized state of the system, respectively, and times are given in minutes. In panel b, we track the spatiotemporal drift of the representative finger marked in panel a. The vertical and horizontal displacement distances are also plotted. (See Supporting Information file list for Figure 1.)

growing convective modes (Figure 1a, lower row) to yield traveling convective fingers thanks to the in situ buoyancy forcing of the flow by the localized oscillatory RD process. The horizontal drift of the finger along the horizontal direction of propagation of the chemical waves indicates the chemical influence on the hydrodynamical pattern. By monitoring the motion of an individual finger, we are able to measure its lateral excursion and vertical displacement, both being in the millimeter scale (see Figure1b). The resulting chemo-hydrodynamic pattern cannot be obtained in the absence of buoyancy flows or without chemical oscillations, as the pulsatile localized chemical and hydrodynamic forcings would then have to be replaced by an external equivalent forcing. This demonstrates the power of RDC self-organization in providing new patterns and instabilities existing only thanks to the synergetic combination of chemical and hydrodynamic modes.

The experimental system consists of a vertical Hele-Shaw (HS) cell, i.e., two rectangular glass plates (35 mm × 70 mm) separated by a gap of 0.25 mm, in which two miscible aqueous solutions containing separate reactants of the bubble free BZ reaction[3] are put in contact along a horizontal line thanks to a specific injection device.[24] Each solution covers half of the reactor height (i.e., 35 mm), featuring a double-layer system. Specifically, we consider the oxidation reaction of CHD (1,4-cyclohexanedione) by bromate, catalyzed by ferroin.[25,26] In a stirred reactor, this reaction produces oscillations while in gels and with an initially homogeneous distribution of all chemicals, traveling waves and spirals can be observed. In the HS cell, the BZ reactants are separated in two solutions: solution 2, of density $\rho_2$ composed of only sulphuric acid, sodium bromate, sodium bromide, and the ferriin ($Fe^{III}$, the catalyst in its oxidized state, blue solution) is put on top of a denser solution 1 of density $\rho_1$ containing only CHD, sulphuric acid and ferroin, (reduced form $Fe^{II}$, red solution). All reactants were commercial grade (Sigma-Aldrich) without any further purification. Slight modifications in the bromate concentrations are considered as a control parameter; nevertheless, in all cases, the upper solution was the less dense one ($\rho_2 < \rho_1$).

A high power LED source was used to illuminate the system. The light path passing through the cell was divided in two by means of a beam splitter. One beam, recorded by a digital camera, gives a direct view of changes in the concentrations, which we call here the "chemical pattern" (Figure 1a, upper row). The second beam is used to get a Schlieren image of gradients in refractive index monitoring convective motions due to related density gradients, images which we refer to as the "hydrodynamic pattern" (Figure 1a, lower row). The field of view of the recorded images was 17.5 mm × 13.7 mm centered between the two solutions. The resolution of both cameras was 720 × 576 pixels at 25 frames per second.

Upon contact between the two solutions, the reactants meet in the miscible contact zone by diffusion where the BZ system starts to oscillate producing horizontal traveling waves, which extend upward and downward in time (Figure 1a). As a control parameter, we vary $[BrO_3^-]$, the initial concentration of bromate, which changes the excitability of the reactive medium. Low values of $[BrO_3^-]$ correspond to low excitability, slow wave propagation, and large wavelengths in the chemical waves (and vice versa).[27] Depending on the excitability, different behaviors were found. For low excitability (Figure 2a), as soon as

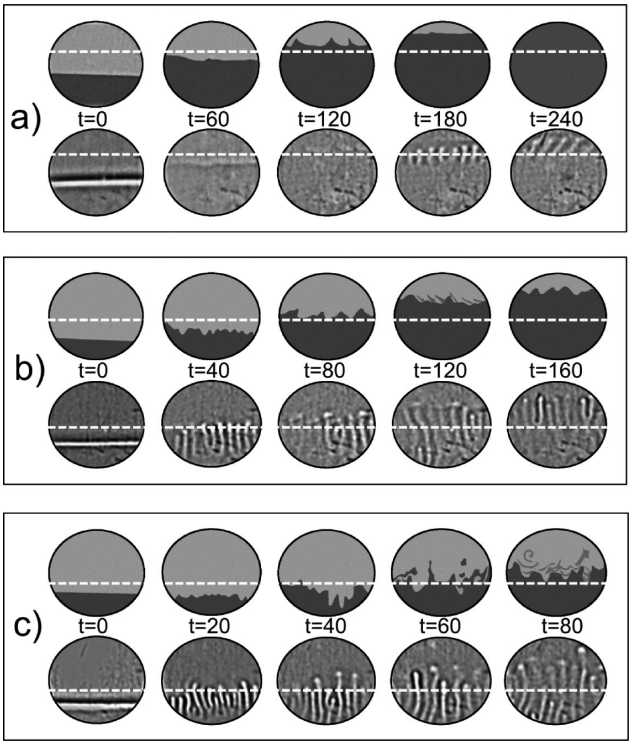


**Figure 2.** Chemical (upper rows of each panel) and hydrodynamic (lower rows of each panel) patterns obtained for increasing values of the initial bromate concentration: $[NaBrO_3]$ = 0.057 M (a), 0.095 M (b), and 0.113 M (c), at successive times given in minutes. The initial concentration of the other chemicals is detailed in ref 25. The white dashed line represent the horizontal cut used for building the space-time plots of Figure 4. (See Supporting Information file list for Figures 2 and 4.)


dx.doi.org/10.1021/jz402625z | J. Phys. Chem. Lett. 2014, 5, 413–418

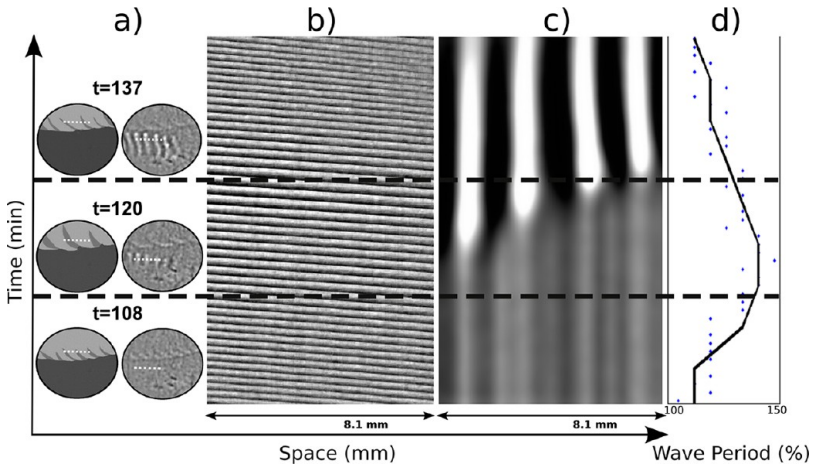


**Figure 3.** Dynamics at three successive times (a) and related space−time plots of the chemical (b) and the hydrodynamic (c) patterns when $[NaBrO_3]$ = 0.066 M. Space−time maps are built by stacking as a function of time the horizontal cut (white dashed line) shown in the experimental frames depicted in panel a, starting at $t$ = 108. (d) Characterization of the chemical wave period changes due to the RDC interplay. (See Supporting Information file list for Figure 3.)

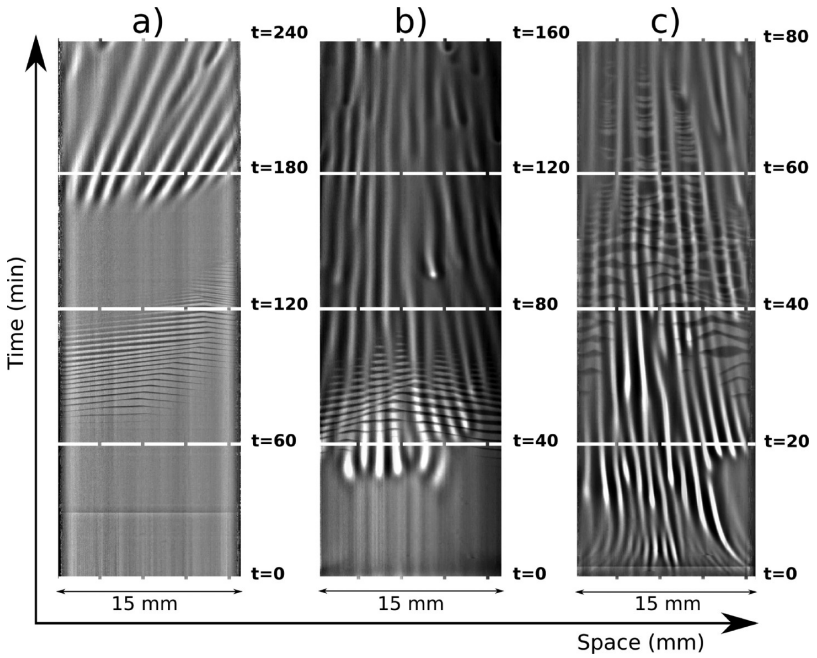


**Figure 4.** Space-time maps superimposing the chemical and the hydrodynamic patterns when $[NaBrO_3]$ = 0.057 M (a), 0.095 M (b), and 0.113 M (c). Horizontal and vertical bright stripes feature the chemical waves and the hydrodynamic fingers dynamics, respectively. Note that as excitability is increased, convective fingers dynamics becomes more complicated as a result of a complex chemical forcing. (See Supporting Information file list for Figures 2 and 4.)

conditions for concentration oscillations are met across the contact zone, some chemical waves start to appear with a large wavelength in the chemical view (upper row), but no convection is seen in the Schlieren view (lower row). Convective cells develop only after a long transient (about 125 min). These convective fingers nucleate at the reactive interface, grow in time along the vertical direction and, importantly, they also move along the horizontal direction in the zone of existence of the chemical waves. The two other cases at larger excitabilities (Figure 2b,c) feature a qualitatively different behavior. The hydrodynamic instability is triggered as soon as chemical waves appear and both chemical and hydrodynamic structures exhibit analogous wavelength. In the high excitability domain (Figure 2c), high rotational flow regions close to the fingers favor the break of the target waves symmetry and the nucleation of small spirals at the interface. For this largest excitability (Figure 2c), the fingers still follow the chemical patterns in the reactive zone, but now the chemical dynamics are more complicated (notice the existence of spiral waves interacting with traveling waves coming from the boundaries), and this is directly reflected in the hydrodynamic pattern.

The scenarios illustrated in Figure 1 and Figure 2 show a clear example of a chemo-hydrodynamic structure in which the final pattern combines properties of the oscillating reaction and of buoyancy-driven instabilities while featuring some new RDC properties like drifting convective cells and characteristic time


dx.doi.org/10.1021/jz402625z | J. Phys. Chem. Lett. 2014, 5, 413−418

and space scales different from those observed in non reactive buoyancy instabilities or in pure RD systems.

Figure 3 shows the space−time plots related to the dynamics as well as quantitative characterization of the wave period as a function of time. The first space-time map (Figure 3b) gives information about the dynamics of the chemical waves shown by the direct view of Figure 3a (left frames), while the second map (Figure 3c) describes the evolution of the hydrodynamic cells as shown by the Schlieren views of Figure 3a (right frames). At the beginning, only chemical waves traveling from the right to the left with a characteristic RD wavelength (4 mm) are present in the system. Once the convective cells are induced (around $t$ = 120 min), they directly affect the chemical wavelength as the reactants are convected by the flows. At the time when the hydrodynamic instability and fingers are well developed, the chemical wave period is increased up to 50% (see Figure 3d), which attests the mutual influence of chemical and transport phenomena. As the concentration field is redistributed by convective motions, it affects in turn the velocity field within the system. After a transient, both chemical and hydrodynamic modes readjust through this feedback into a new chemo-hydrodynamic pattern with a characteristic constant wavelength and constant velocity.

Figure 4 presents the space−time plots characterizing the transition from simple to complex chemo-hydrodynamic behaviors for increasing $[BrO_3^-]$. Here the superimposition of the chemical and the Schlieren views allows one to appreciate the correlation between the chemical and hydrodynamic patterns seen in Figure 2. Figure 4a describes a relatively low excitable system where a long-wavelength train of waves moves here from left to right. In Figure 4b,c, the excitability of the system is quite high, and chemical waves exhibit complicated patterns with a competition between target and spiral waves coming from different directions which collide in the mixing zone. As a result, the hydrodynamic pattern, closely following the chemical dynamics, exhibits an intricate behavior that actually changes with time.

The chemo-hydrodynamic structures can be characterized by the characteristic wavelengths of the chemical and hydrodynamic patterns respectively. First, the chemical wavelength $\lambda_c$ of the localized drifting concentration waves seen in the direct view is obtained as the distance between two successive concentration extrema at a given time. The second characteristic spatial scale is the hydrodynamic wavelength $\lambda_h$ of the convective structure obtained thanks to a Fourier transform of the Schlieren convective pattern. We see on Figure 5a that $\lambda_h$ remains roughly constant and of the order of 1.5 mm independently of the excitability. A third wavelength, $\lambda_P$ is the characteristic reaction-diffusion wavelength of the waves obtained in a separate Petri dish by mixing homogeneously all reactants with the same chemical composition as in the reacting zone. Note that for low values of bromate concentrations, $\lambda_c$ and $\lambda_P$ differ due to the different initial condition and the large dispersity of wavelengths compatible with these concentration values. As excitability is increased, this difference is diminished and exhibit the minimum value accessible by the system. The direct comparison between the chemical $\lambda_c$ and hydrodynamic $\lambda_h$ scalings (Figure 5a) shows how, at low bromate concentration, $\lambda_c$ is much larger as the traveling concentration waves are roughly 3 times larger than the convective cells. This difference vanishes at larger excitability ($[BrO_3^-] \geq 0.085$ M) where both $\lambda_c$ and $\lambda_h$ converge to the homogeneous reaction-diffusion wavelength

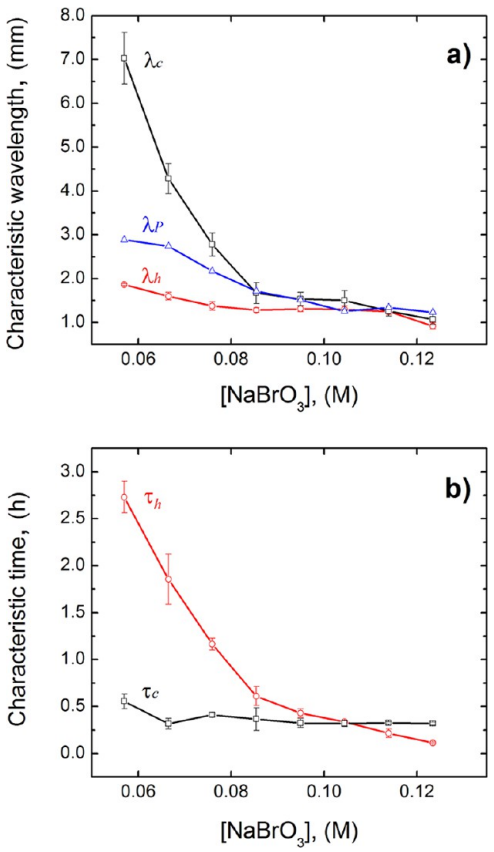


**Figure 5.** (a) Chemical ($\lambda_c$) and hydrodynamic ($\lambda_h$) wavelengths as a function of $[NaBrO_3]$, as compared to the RD wavelength, $\lambda_p$. (b) Dependence of the onset time of the chemical and hydrodynamic patterns upon $NaBrO_3$ concentration. Solid lines are just a guide for the eyes.

$\lambda_P$, which is around 1.5 mm. The onset times, $\tau_h$ of the convective modes and $\tau_c$ of the chemical pattern also vary with the excitability as shown on Figure 5b. At low excitability, convective patterns appear much later than the traveling waves, while they develop on the same time scale ($\tau_h \sim \tau_c$) when the system is more excitable ($[BrO_3^-] \geq 0.085$ M). Note that for the largest value of bromate concentration, the hydrodynamic instability occurs before the wave instability. This suggests that chemical species involved in the convective mechanism appear then on a time scale faster than the time needed for chemical waves to develop.

In order to gain insight into the instability mechanism at the origin of the convection, we recall that, in such reactive systems, convective fingers are either due to a Rayleigh−Taylor (RT) instability when a denser solution overlies a less dense one[13,28] or to a differential diffusion mechanism when a statically stable density stratification is destabilized because of the contribution to the density of various solutes diffusing at different rates.[6,13,28] We have performed several experiments varying the composition of the solutions to test some instability scenarios. However, in all cases, $\rho_2 < \rho_1$ to exclude an RT instability. First, similar experiments have been performed with an equal concentration of acid in both layers. No qualitative difference is obtained, and only the quantitative values of the excitability at which complex phenomena come into play is slightly shifted. This rules out that convection is due to double diffusion triggered by a larger amount of fast diffusive protons in the lower layer. A difference in diffusivity between the oxidized and reduced forms of the


dx.doi.org/10.1021/jz402625z | J. Phys. Chem. Lett. 2014, 5, 413−418

catalyst independently of the oscillatory mechanism is also excluded because convection appears as well using the uncatalyzed Bromate-CHD oscillator,[29] which oscillates even in the absence of the catalyst. Convective fingers are then present in the Schlieren view even if the absence of a color change due to the absence of ferroin does not allow one to follow the concentration dynamics. This convection develops on a slower time scale than in the presence of ferroin indicating that the $Fe^{II}/Fe^{III}$ species, although not essential to the chemo-hydrodynamic coupling studied here, can nevertheless influence its time scale by changing the oscillatory mechanism.

If we next keep the ferroin catalyst but redo the experiment without any CHD in the lower layer, no oscillations are obtained, and the dynamics solely consists in a chemical planar oxidation front invading the lower layer, showing that CHD is an essential ingredient in the instability mechanism. Similarly, if chloride ions, known to inhibit the BZ oscillations,[30,31] are introduced into the system convective motions are gradually suppressed. This points to the necessity to preserve the oscillatory mechanism in the reaction zone to obtain convection. We conjecture that the instability arises from a chemically driven double-diffusion mechanism localized at the reactive region, where oscillations in time and space of intermediate species trigger pulsatile density gradients at the origin of the traveling convective fingers. Note that the existence of the reaction in the system is crucial in order to induce the double-diffusion instability. The most probable candidates seem to be the brominated organic substrate, BrCHD, and the heat released during the "resetting of the chemical clock" step, which is proportional to the organic component of the BZ-like systems and to the catalyst concentration.[32] Differential diffusivity is expected both from an increase of the molecular mass of the intermediate organic species and from heat diffusion, which is much faster than the mass one. Once these key variables reach a critical value, a hydrodynamic instability is promoted, resulting in convective fingers. As the initial concentration of $BrO_3^-$ is small, the diffusion-controlled chemical feeding supplied from the upper solution and the reaction kinetics are slow, thus the intermediate reactants are not produced immediately in sufficient amounts, and $\tau_h > \tau_c$. For a high excitability, the density jump between the upper and the lower layer is decreased, the intermediates formation is readily enhanced, and, consequently, the induction period for the onset of the convective instability drops down to $\tau_h \sim \tau_c$, as shown in Figure 5b.

To summarize, we have presented here the evidence of a self-organized traveling chemo-hydrodynamic structure resulting from an in situ hydrodynamic instability sustained by an oscillating reaction at the miscible interface between two solutions containing initially separated reactants of the BZ reaction. This particular configuration induces a transverse coupling among horizontally traveling waves and vertically growing convective fingers. Future work will need to compare modeling of related RDC models to further experiments devoted to decipher the role of the various chemical intermediates that could be responsible for the observed phenomena. These results pave the way to more studies devoted to unravel new self-organized RDC instability scenarios due to the intimate coupling of reaction and convective phenomena.

## ■ ASSOCIATED CONTENT

### Ⓢ Supporting Information

We include within this Supporting Information the experimental video records of the results used for the creation of Figures 1−4. All movies presented here are accelerated 100 times the original velocity. The frame size is 17.5 mm × 13.7 mm. Files for Figure 1: **1a_Chem_0.085M.avi** (corresponds to the chemical patterns of Figure 1a and $[BrO_3^-]$ = 0.085 M), **1a_Hydro_0.085M.avi** (corresponds to the hydrodynamic patterns of the Figure 1a and $[BrO_3^-]$ = 0.085 M), and **1b_Finger_Tracking_0.085M.avi** (corresponds to the motion tracking of the hydrodynamic finger of the Figure 1b). Files for Figures 2 and 4: **2a_4a_Chem_0.057M.avi** (corresponds to the chemical patterns of Figure 2a and with the space time plot of Figure 4a. $[BrO_3^-]$ = 0.057 M), **2a_4a_Hydro_0.057M.avi** (corresponds to the hydrodynamic patterns of Figure 2a and with the space time plot of Figure 4a. $[BrO_3^-]$ = 0.057 M), **2b_4b_Chem_0.095M.avi** (corresponds to the chemical patterns of Figure 2b and with the space time plot of Figure 4b. $[BrO_3^-]$ = 0.095 M), **2b_4b_Hydro_0.095M.avi** (corresponds to the hydrodynamic patterns of Figure 2b and with the space time plot of Figure 4b. $[BrO_3^-]$ = 0.095 M), **2c_4c_Chem_0.113M.avi** (corresponds to the chemical patterns of Figure 2c and with the space time plot of Figure 4c. $[BrO_3^-]$ = 0.113 M), and **2c_4c_Hydro_0.113M.avi** (corresponds to the hydrodynamic patterns of Figure 2c and with the space time plot of Figure 4c. $[BrO_3^-]$ = 0.113 M). Files for Figure 3: **3a_3b_Chem_0.066M.avi** (this file was used to construct the frames of Figure 3a and the time space plot of Figure 3b. $[BrO_3^-]$ = 0.066 M) and **3a_3c_Hydro_0.066M.avi** (this file was used to construct the frames of Figure 3a and the time space plot of Figure 3c. $[BrO_3^-]$ = 0.066 M). This material is available free of charge via the Internet at http://pubs.acs.org/.

## ■ AUTHOR INFORMATION


### Corresponding Authors

*E-mail: dmescala@gmail.com.
*E-mail: mabudroni@uniss.it.
*E-mail: jorge.carballido@gmail.com.
*E-mail: adewit@ulb.ac.be.
*E-mail: alberto.perez.munuzuri@usc.es.

### Present Addresses

[§](M.A.B.) Dipartimento di Chimica e Farmacia, Università di Sassari, Via Vienna 2, Sassari 07100 - Italy.
[⊥](J.C.-L.) Department of Earth and Planetary Sciences, Harvard University, Cambridge, Massachusetts, USA.


### Notes

The authors declare no competing financial interest.

## ■ ACKNOWLEDGMENTS

This work was supported by Xunta de Galicia under Research Grant No. CN2012/315 and a Predoctoral Grant (D.M.E.). We acknowledge financial support from FNRS-FORECAST and Prodex (A.D.) as well as the Regione Sardegna POR project (M.A.B.).

## ■ REFERENCES

(1) Cross, M. C.; Hohenberg, P. C. Pattern Formation Outside of Equilibrium. *Rev. Mod. Phys.* **1993**, *65*, 851−1112.
(2) Kapral, R.; Showalter, K. *Chemical Waves and Patterns*; Kluwer Academic Publishers: Dordrecht, The Netherlands, 1995.

(3) Pojman, J. A.; Epstein, I. R. *An Introduction to Nonlinear Chemical Dynamics Oscillations, Waves, Patterns and Chaos*; Oxford University Press: New York, 1998.
(4) De Wit, A.; Eckert, K.; Kalliadasis, S. Introduction to the Focus issue: Chemo-hydrodynamic Patterns and Instabilities. *Chaos* **2012**, *22*, 037101.
(5) Eckert, K.; Grahn, A. Plume and Finger Regimes Driven by an Exothermic Interfacial Reaction. *Phys. Rev. Lett.* **1999**, *82*, 4436−4439.
(6) Almarcha, C.; Trevelyan, P. M. J.; Grosfils, P.; De Wit, A. Chemically Driven Hydrodynamic Instabilities. *Phys. Rev. Lett.* **2010**, *104*, 044501.
(7) von Kameke, A.; Huhn, F.; Fernández-García, G.; Muñuzuri, A. P.; Pérez-Muñuzuri, V. Double Cascade Turbulence and Richardson Dispersion in a Horizontal Fluid Flow Induced by Faraday Waves. *Phys. Rev. Lett.* **2011**, *107*, 074502.
(8) Neufeld, Z.; Hernández-García, E. *Chemical and Biological Processes in Fluid Flows: A Dynamical Systems Approach*; Imperial College Press: London, 2010.
(9) Vladimirova, N.; Rosner, R. Model Flames in the Boussinesq Limit: The Case of Pulsating Fronts. *Phys. Rev. E* **2005**, *71*, 067303.
(10) Belk, M.; Kostarev, K. G.; Volpert, V.; Yudina, T. M. Frontal Photopolymerization with Convection. *J. Phys. Chem. B* **2003**, *107*, 10292−10298.
(11) Avnir, D.; Kagan, M. Spatial Structures Generated by Chemical Reactions at Interfaces. *Nature* **1984**, *307*, 717−720.
(12) Andres, J. T. H.; Cardoso, S. S. S. Onset of Convection in a Porous Medium in the Presence of Chemical Reaction. *Phys. Rev. E* **2011**, *83*, 046312.
(13) Lemaigre, L.; Budroni, M. A.; Riolfo, L. A.; Grosfils, P.; De Wit, A. Asymmetric Rayleigh-Taylor and Double-Diffusive Fingers in Reactive Systems. *Phys. Fluids* **2013**, *25*, 014103.
(14) Nagy, I. P.; Keresztessy, A.; Pojman, J. A. Periodic Convection in the Bromate−Sulfite Reaction: A "Jumping" Wave. *J. Phys. Chem.* **1995**, *99*, 5385−5388.
(15) Komlosi, A.; Nagy, I. P.; Pojman, J. A. Convective Chemical Fronts in the 1,4-Cyclohexanedione-Bromate-Sulfuric Acid-Ferroin System. *J. Phys. Chem.* **1998**, *102*, 9136−9141.
(16) Keresztessy, A.; Nagy, I. P.; Bazsa, G.; Pojman, J. A. Traveling Waves in the Iodate-Sulfite and Bromate-Sulfite Systems. *J. Phys. Chem.* **1995**, *99*, 5379−5384.
(17) D'Hernoncourt, J.; Zebib, A.; De Wit, A. Reaction Driven Convection Around a Stably Stratified Chemical Front. *Phys. Rev. Lett.* **2006**, *96*, 154501.
(18) Schuszter, G.; Tóth, T.; Horváth, D.; Tóth, Á. Convective Instabilities in Horizontally Propagating Vertical Chemical Fronts. *Phys. Rev. E* **2009**, *79*, 016216.
(19) Miike, H.; Müller, S. C.; Hess, B. Oscillatory Deformation of Chemical Waves Induced by Surface Flow. *Phys. Rev. Lett.* **1988**, *61*, 2109−2112.
(20) Miike, H.; Yamamoto, H.; Kai, S.; Müller, S. C. Accelerating Chemical Waves Accompanied by Traveling Hydrodynamic Motion and Surface Deformation. *Phys. Rev. E* **1993**, *48*, R1627−R1630.
(21) Yoshikawa, K.; Kusumi, T.; Ukitsu, M.; Nakata, S. Generation of Periodic Force with Oscillating Chemical Reaction. *Chem. Phys. Lett.* **1993**, *211*, 211−213.
(22) Budroni, M. A.; Rongy, L.; De Wit, A. Dynamics due to Combined Buoyancy- and Marangoni-Driven Convective Flows Around Autocatalytic Fronts. *Phys. Chem. Chem. Phys.* **2012**, *14*, 14619−14629.
(23) Rossi, F.; Budroni, M. A.; Marchettini, N.; Carballido-Landeira, J. Segmented Waves in a Reaction−Diffusion−Convection System. *Chaos* **2012**, *22*, 037109−037109.
(24) Shi, Y.; Eckert, K. A Novel Hele-Shaw Cell Design for the Analysis of Hydrodynamic Instabilities in Liquid−Liquid Systems. *Chem. Eng. Sci.* **2008**, *63*, 3560−3563.
(25) Solution 1 (15 mL): 4.40 mL $H_2SO_4$ 6.35 M, 5.46 mL CHD 0.8 M, 0.28 mL Ferroin 0.025 M, and 4.86 mL $H_2O$. Solution 2 (15 mL): 3.67 mL $H_2SO_4$ 6.35 M, 1.42 mL [0.6:1.3] M $NaBrO_3$, 0.47 mL NaBr 1 M, 0.20 mL Ferroin 0.025 M, and 9.24 mL $H_2O$.
(26) Kurin-Csörgei, K.; Zhabotinsky, A. M.; Orbán, M.; Epstein, I. R. Bromate-1, 4-Cyclohexanedione-Ferroin Gas-Free Oscillating Reaction. 1. Basic Features and Crossing Wave Patterns in a Reaction−Diffusion System without Gel. *J. Phys. Chem.* **1996**, *100*, 5393−5397.
(27) Muñuzuri, A.; Gómez-Gesteira, M.; Perez-Muñuzuri, V.; Krinsky, V.; Pérez-Villar, V. Parametric Resonance of a Vortex in an Active Medium. *Phys. Rev. E* **1994**, *50*, 4258−4261.
(28) Trevelyan, P. M. J.; Almarcha, C.; De Wit, A. Buoyancy-Driven Instabilities of Miscible Two-Layer Stratifications in Porous Media and Hele-Shaw Cells. *J. Fluid Mech.* **2011**, *670*, 38−65.
(29) Szalai, I.; Kurin-Csörgei, K.; Epstein, I. R.; Orban, M. Dynamics and Mechanism of Bromate Oscillators with 1,4-Cyclohexanedione. *J. Phys. Chem. A* **2003**, *107*, 10074−10081.
(30) Kurin-Csörgei, K.; Nagy, G.; Körös, E. Temperature-Triggered Chemical Oscillators. A Peculiar Temperature Effect in Perturbed Uncatalyzed Bromate-Driven Reactions. *Chem. Phys. Lett.* **1997**, *271*, 67−72.
(31) Jacobs, S. S.; Epstein, I. R. Effects of Chloride Ion on Oscillations in the Bromate-Cerium-Malonic Acid System. *J. Am. Chem. Soc.* **1976**, *98*, 1721−1724.
(32) Pojman, J. A.; Epstein, I. R. Convective Effects on Chemical Waves. 1. Mechanisms and Stability Criteria. *J. Phys. Chem.* **1990**, *94*, 4966−4972.